

**Table 1.** Mean survival and tumor induction in male mice

Group	Effective animal	Mean survival (Days)	Tumor bearing animals (%)	No of tumor /mouse	Liver			Lung (%)	Other (%)
					Incidence (%)	No / mouse	Size (mm)		
0.18 MeV	30	407 ± 25	16(53)*	0.53 ± 0.50**	10(33)*	0.43 ± 0.73	3.33±6.56	4(13)	2(7)
0.32 MeV	26	412 ± 10	13(50)*	0.54 ± 0.58**	8(31)*	0.38 ± 0.64	3.21±3.52	3(12)	3(12)
0.60 MeV	30	410 ± 6	18(60)*	0.70 ± 0.75**	12(40)*	0.57 ± 0.82** <sup>a</sup>	4.07±7.28*	2(7)	8(27)*
1.0 MeV	30	414 ± 6	13(43)*	0.43 ± 0.50*	5(17)*	0.20 ± 0.48 <sup>a</sup>	0.95±2.93	2(7)	6(20)*
Control	36	413 ± 2	4(11)	0.11 ± 0.32	4(11)	0.11 ± 0.32	0.81±2.64	0	0

Mean ± SD

\*: Significantly different from Control value (P &lt; 0.05)

\*\*: Significantly different from Control value (P &lt; 0.01)

<sup>a</sup>: Significantly different between 0.6 MeV and 1.0 MeV (P < 0.05)**Table 2.** Numbers of histological typing tumors of male mice

Group (MeV)	Liver		Lung		Other	
	Hepatoma	Hepatocellular - carcinoma	Adenoma	Adeno - carcinoma	No	Tumor type
0.18	12	1	3	1	2	Harderian gland adenoma 1 Bone osteosarcoma 1
0.32	10	0	1	2	3	Harderian gland adenoma 1 Bone osteosarcoma 1 Skin papilloma 1
0.6	17	0	0	2	8	Harderian gland adenoma 2 Pituitary adenocarcinoma 2 Leukemia 1 Muscle sarcoma 2 Adrenal cortical adenoma 1
1.0	6	0	2	0	6	Harderian gland adenoma 3 Pituitary adenoma 1 Skin papilloma 2
Control	5	0	0	0	0	

body weights among the female groups. Uterus weights in all irradiated groups were significantly decreased as compared to the control values, whereas adrenal weights increased in 0.18 MeV group (relative to both control and 1.0 MeV groups). Relative liver weights at 0.32 and 0.6 MeV and kidney weights at 0.32 MeV were significantly higher than control values while weights of adrenals at 1.0 MeV and spleen at 0.6 MeV were significantly decreased as compared to the 0.18 MeV values (data not shown).

Tumors were found in 71% to 85% of animals in the irra-

diated groups, with mean incidences of 1.27 to 1.56 tumors per animal (see Table 3). The highest incidences were noted for tumors of the ovary (41–54%), followed by the Harderian glands. There were no significant differences among the radiation groups. From histopathological findings, radiation-induced tumors were rather low in malignancy (Table 4). However, 3, 3, 1, and 6 malignant granulosa cell tumors in the ovary were observed at 0.18, 0.32, 0.6 and 1.0 MeV, respectively, and three had metastasized to the lungs in the 1.0 MeV group.

**Table 3.** Mean survival and tumor induction in female mice

	Effective No	Mean survival (Days)	Total (%)	No of tumor / mouse	Ovary (%)	Lung (%)	Liver (%)	Harderian Gland (%)	Lymphoma (%)	Others (%)
0.18 MeV	28	412 ± 35	22(79)*	1.32 ± 0.47*	19(68)*	1(4)	4(14)	2(7)	2(7)	2(7)
0.32 MeV	27	410 ± 49	22(81)*	1.27 ± 0.55*	18(67)*	2(7)	1(4)	3(11)	1(4)	4(15)
0.6 MeV	28	421 ± 17	23(82)*	1.38 ± 0.57*	15(54)*	3(11)	4(14)	7(25)*	0	6(21)*
1.0 MeV	27	408 ± 52	25(93)*	1.56 ± 0.83*	15(56)*	1(4)	7(26)	6(22)*	2(7)	2(7)
Control	36	427 ± 1	0	0	0	0	0	0	0	0

Mean ± SD

\*: Significantly different from Control value (P &lt; 0.05)

**Table 4.** Number of histological typing tumors in male mice

Group (MeV)	Ovary			Lung		Liver		Harderian gland		Others	
	Tubulostomal adenoma	Benign granulosa cell tumor	Malignant granulosa cell tumor	Adenoma	Adeno-carcinoma	Hepatoma	Hepatocellular-carcinoma	Adenoma	Adeno-carcinoma	No	
0.18	13	3	3	0	1	3	0	2	0	2	Adrenal cortical adenoma 1 Lymphoma 1
0.32	10	5	3	0	1	2	1	2	1	4	Muscle sarcoma 1 Pituitary adenoma 3
0.6	9	5	1	1	0	3	1	5	2	6	Pituitary adenoma 1 Uterus endometrial tumor 1 Muscle sarcoma 1 Skin papilloma 1 Adrenal cortical adenoma 2
1.0	6	6	6	1	0	4	3	5	1	2	Skin squamous cell carcinoma 1 Mammary adenocarcinoma 1
Control	0	0	0	0	0	0	0	0	0	0	

## DISCUSSION

In the present study, there were no consistent differences in tumor incidence among the groups with various energies of neutron irradiation. In males, the incidence, number and size of liver tumors were significantly increased in irradiated animals as compared with non-irradiated controls, but without significant differences among the irradiated groups. In females, some tumors in the irradiated groups were significantly more common than in their non-irradiated counterparts but again there was no significant variation with the dose applied. Induced tumor incidences in males were 43%–60% and in females were 79%–93%. Takahashi *et al.*<sup>15</sup> reported an incidence of 46.7% (hepatic tumors 43.3%) in B6C3F1 male mice and 23.3% in females receiving 50 cGy of <sup>252</sup>Cf neutrons, while we<sup>16</sup> reported tumor incidences of

30% in both sexes of mice receiving 42.5 cGy of 290 MeV/u carbon-iron irradiation. In males, the tumor incidence seems to be the same between <sup>252</sup>Cf neutrons and monoenergetic neutrons but the incidence of tumors after heavy-iron irradiation was less than that after neutrons in the present experiment. In females, the tumor incidence in the present experiment was higher than with <sup>252</sup>Cf neutrons.

Inverse dose-rate dependence of fission-spectrum neutron induction on somatic *hprt* mutations in mouse leukemia L5178Y cells has been reported by Nakamura and Sawada<sup>10</sup>, Hill *et al.* observed that reduction of the dose rate of fission neutrons increased their effectiveness for transformation of C3H 10T1/2 cells.<sup>17,18</sup> Brenner and Hall published a model of an inverse dose-rate effect for neoplastic transformation *in vitro* following high LET irradiation.<sup>19</sup> Harrison and Bakcer-Kubiczek *et al.*, however, found modification of fission neutron dose-response curves by dose rate

to be negligible or absent.<sup>20, 21)</sup> Watanabe *et al* reported that a single <sup>252</sup>Cf neutron dose resulted in higher incidences of ovarian and Harderian gland tumors than the same total dose given at a low dose rate with B6C3F1 mouse whole body irradiation.<sup>22)</sup> Clearly there may be differences in dose-rate effect between the *in vitro* and *in vivo*. It is considered that cells with large chromosomal aberrations or other abnormalities might be able to survive *in vitro*, but *in vivo* they might not, so smaller non-lethal chromosomal changes such as point mutations, frame shifts, as small insertions or deletions could be essential for tumor induction *in vivo*. The source of irradiation, strain, sex, and age are all clearly the factors, which need to be taken into account when determining radiation sensitivity. The reason why tumor incidences in mice were not influenced by the various neutron energies is not understood; however, Sasaki *et al*<sup>23)</sup> recently reported that induction of chromosome aberrations is not largely dependent on neutron energy. Further studies on different biologic endpoints are required to address this issue.

In conclusion, there were no consistent differences in tumor incidence among the various energies of neutron irradiation applied.

#### ACKNOWLEDGEMENTS

We are grateful to Dr. Malcolm A. Moore for reading the manuscript and Mr. T. Nishioka for his technical assistance.

#### REFERENCES

1. Miller, R. C., Geard, C. R., Brenner, D. J., Komatsu, K., Marino, S. A. and Hall, E. J. (1989) Neutron-energy-dependent oncogenic transformation of C3H 10T1/2 mouse cells. *Radiat. Res.* **117**: 114–127.
2. Miller, R. C., Marino, S. A., Martin, S. G., Komatsu, K., Geard, C. R., Brenner, D. J. and Hall, E. J. (1999) Neutron-energy-dependent cell survival and oncogenic transformation. *J. Radiat. Res. (Tokyo)*. **40** Suppl: 53–59.
3. Pandita, T. K. and Geard, C. R. (1996) Chromosome aberrations in human fibroblasts induced by monoenergetic neutrons. I. Relative biological effectiveness. *Radiat. Res.* **145**: 730–739.
4. Tanaka, K., Gajendiran, N., Endo, S., Komatsu, K., Hoshi, M. and Kamada, N. (1999) Neutron energy-dependent initial DNA damage and chromosomal exchange. *J. Radiat. Res. (Tokyo)*. Suppl: 36–44.
5. Tanaka, K., Kobayashi, T., Sakurai, Y., Nakagawa, Y., Endo, S. and Hoshi, M. (2001) Dose distributions in a human head phantom for neutron capture therapy using moderated neutrons from the 2.5 MeV proton-<sup>7</sup>Li reaction or from fission of <sup>235</sup>U. *Phys Med Biol.* **46**: 2681–2695.
6. Zhang, W., Fujikawa, K., Endo, S., Ishikawa, M., Ohtaki, M., Ikeda, H. and Hoshi, M. (2003) Energy-dependent RBE of neutrons to induce micronuclei in root-tip cells of *Allium cepa* onion irradiated as dry dormant seeds and seedlings. *J. Radiat. Res. (Tokyo)*. **44**: 171–177.
7. Gajendiran, N., Tanaka, K. and Kamada, N. (2000) Comet assay to sense neutron 'fingerprint'. *Mutat. Res.* **452**: 179–187.
8. Gajendiran, N., Tanaka, K., Kumaravel, T. S. and Kamada, N. (2001) Neutron-induced adaptive response studied in G0 human lymphocytes using the comet assay. *J. Radiat. Res. (Tokyo)*. **42**: 91–101.
9. Kubota, N., Okada, S., Nagatomo, S., Ozawa, F., Inada, T., Hill, C. K., Endo, S. and Komatsu, K. (1999) Mutation induction and RBE of low energy neutrons in V79 cells. *J. Radiat. Res. (Tokyo)*. **40** Suppl: 21–27.
10. Nakamura, N. and Sawada, S. (1988) Reversed dose-rate effect and RBE of 252-californium radiation in the induction of 6-thioguanine-resistant mutations in mouse L5178Y cells. *Mutat. Res.* **201**: 65–71.
11. Schmid E., Schlegel D., Guldbakke S., Kapsch R. P. and Regulla D. (2003) RBE of nearly monoenergetic neutrons at energies of 36 keV-14.6 MeV for induction of dicentric in human lymphocytes. *Radiat. Environ Biophys.* **42**: 87–94.
12. Endo, S., Hoshi, M., Tauchi, H., Takeoka, S., Kitagawa, K., Suga, S., Maeda N., Komatsu, K., Sawada, S., Iwamoto, E., Sakamoto, S., Takeyama, K. and Omura, M. (1995) Neutron generator at Hiroshima University for use in radiobiology study. *J. Radiat. Res. (Tokyo)*. **36**: 91–102.
13. Endo, S., Hoshi, M., Takada, J., Tauchi, H., Matsuura, S., Takeoka, S., Kitagawa, K., Suga, S. and Komatsu, K. (1999) Neutron generator (HIRRAC) and dosimetry study. *J. Radiat Res (Tokyo)*. **40** Suppl: 14–20
14. Lee C. L. and Zhou X. L. (1999) Thick target neutron yields for the <sup>7</sup>Li(p, n)<sup>7</sup>Be reaction near threshold. *Nucl. Instrum. Methods Phys. Res. B* **152**: 1–11.
15. Takahashi, T., Watanabe, H., Dohi, K. and Ito, A. (1992) <sup>252</sup>Cf relative biological effectiveness and inheritable effects of fission neutrons in mouse liver tumorigenesis. *Cancer Res.* **52**: 1943–1953.
16. Watanabe, H., Ogiu, T., Nishimura, M., Masaoka, Y., Kusumi, M., Takahashi, T., Oruri, T., Shoji, S. and Katoh, O. (1998) Comparison of tumorigenesis between accelerated heavy ions and X-rays in B6C3F1 mice. *J. Radiat. Res. (Tokyo)*. **39**: 93–100.
17. Hill, C. K., Han, A. and Elkind, M. M. (1984) Fission-spectrum neutrons at a low dose rate enhance neoplastic transformation in the linear, low dose region (0–10 cGy). *Int. J. Radiat. Biol. Relat. Stud. Phys. Chem. Med.* **46**: 11–15.
18. Hill C. K. and Williams-Hill D. (1999) Neutron carcinogenesis: past, present, and future. *J. Radiat. Res. (Tokyo)*. **40** Suppl: 117–127.
19. Brenner, D. J. and Hall, E. J. (1990) The inverse dose-rate effect for oncogenic transformation by neutrons and charged particles: a plausible interpretation consistent with published data. *J. Radiat. Biol.* **58**: 745–758.
20. Harrison, G. H. and Balcer-Kubiczek, E. K. (1992) Ambiguity of the Brenner-Hall model. *Int. J. Radiat. Biol.* **61**: 139–143.
21. Balcer-Kubiczek, E. K., Harrison, G. H., Hill, C. K. and Blakely, W. F. (1993) Effects of WR-1065 and WR-151326 on survival and neoplastic transformation in C3H/10T1/2 cells exposed to TRIGA or JANUS fission neutrons. *Int. J. Radiat. Biol.* **63**: 37–46.
22. Watanabe, H., Okamoto, T., Yamada, K., Ando, Y., Ito, A.,

- Hoshi, M. and Sawada, S. (1993) Effects of dose rate and energy level on fission neutron ( $^{252}\text{Cf}$ ) tumorigenesis in B6C3F1 mice. *J. Radiat. Res. (Tokyo)*. **34**: 235–239.
23. Sasaki, M. S., Endo, S., Ejima, Y., Saito, I., Okamura, K., Oka, Y. and Hoshi, M. (2006) Effective dose of A-bomb radiation in Hiroshima and Nagasaki as assessed by chromosomal effectiveness of spectrum energy photons and neutrons. *Radiat. Environ. Biophys.* **45**: 79–91.

*Received on February 20, 2006*

*1st Revision received on July 25, 2006*

*2nd Revision received on December 18, 2006*

*3rd Revision received on February 27, 2007*

*Accepted on February 28, 2007*

*J-STAGE Advance Publication Date: April 19, 2007*

## Pathological Changes in the Gastrointestinal Tract of a Heavily Radiation-exposed Worker at the Tokai-mura Criticality Accident

Hiroshi IGAKI<sup>1</sup>, Keiichi NAKAGAWA<sup>1\*</sup>, Hiroshi UOZAKI<sup>2</sup>, Masaaki AKAHANE<sup>1</sup>, Yoshio HOSOI<sup>1,3</sup>, Masashi FUKAYAMA<sup>2</sup>, Kiyoshi MIYAGAWA<sup>3</sup>, Makoto AKASHI<sup>4</sup>, Kuni OHTOMO<sup>1</sup> and Kazuhiko MAEKAWA<sup>5</sup>

**Acute radiation exposure/Criticality accident/Multiple organ dysfunction syndrome/Gastrointestinal syndrome.**

Gastrointestinal syndrome after high-dose acute radiation whole body exposure is difficult to treat, although it is a well-known complication. In this report, we describe the clinical and pathological features of a patient who died after the criticality accident which occurred in Japan on 30 September 1999. The patient was estimated to have been exposed to 16–25 Gy equivalent of gamma ray, and died of multiple organ failure after acute radiation syndrome, especially gastrointestinal syndrome, on day 82. The stomach and small intestine contained a large amount of blood clots and the gastrointestinal epithelial cells were almost totally depleted at autopsy. In addition, the degree of the mucosal damage was dependent on the segment of the gastrointestinal tract; the mucosa of stomach, ileum and ascending colon was entirely depleted, but the esophagus, descending and sigmoid colon and rectum retained a small portion of the epithelial cells. From the posture of the patient at the time of exposure, the absorbed dose was presumed to be highest in the right-anterior abdomen. This agreed with the pathological differences in the mucosal damage by the position in the abdomen, which depended presumably on the radiation dose. This is the first report documenting the relationship between the absorbed dose and the severity of gastrointestinal damages *in vivo*.

### INTRODUCTION

Patients suffering from accidental acute radiation exposure are often difficult to treat for several reasons: the difficulty and uncertainty of estimating the exposure dose, the heterogeneity of the absorbed dose in the body, the scarcity of medical staff who are well acquainted and experienced with the treatment of radiation damage to the organs, and the lack of sufficient human data on acute radiation damage to the organs after a single high-dose radiation exposure.<sup>1)</sup>

Recent studies have revealed the close relationship between acute radiation syndrome and multiple organ dysfunction syndrome (MODS) or multiple organ failure (MOF).<sup>2,3)</sup>

Moreover, the gastrointestinal tract plays an important role in developing MODS by the collapse of the intestinal barrier function from enteric bacterium after radiation exposure as well as after severe burns or other trauma.<sup>3,4)</sup>

The criticality accident occurred at the uranium fuel processing facility of JCO Co. Ltd. in Tokai-mura, Ibaraki, Japan in 1999. Two workers were pouring uranyl nitrate solution manually from a bucket into a precipitation tank, when the tank reached the critical state. Three workers received mixed gamma ray and neutron beam. Two of the victims died due to radiation damage. In this report, we focused on the gastrointestinal syndrome of the patient who was exposed most heavily and was treated at our hospital. We present the clinical course and pathological findings related to the irradiation damage in the patient's gastrointestinal tract.

### MATERIALS AND METHODS

#### *Clinical course of the patient*

The patient was 35-year-old male. The patient's exposure was estimated to be a systemic mean dose of 16–25 Gy equivalent of gamma ray by the criticality accident at JCO

\*Corresponding author: Phone: +81-3-5800-8666,

Fax: +81-3-5800-8935,

E-mail: nakagawa-rad@umin.ac.jp

Departments of <sup>1</sup>Radiology, <sup>2</sup>Pathology, and <sup>3</sup>Radiation Biology, University of Tokyo Hospital, Tokyo, Japan; <sup>4</sup>Division of Radiation Health, National Institute of Radiological Sciences, Chiba, Japan; <sup>5</sup>Kanto Central Hospital, Tokyo, Japan.

doi:10.1269/jrr.07058

Co., Ltd., an uranium fuel processing plant in Tokai-mura, Ibaraki, Japan, on 30 September 1999.<sup>6)</sup> He was transferred from the National Institute of Radiological Sciences to the University of Tokyo Hospital on day 2. After his admission at our hospital, continuous intravenous administration of L-alanyl-L-glutamine was started expecting promotion of the epithelial regeneration of the gastrointestinal tract after radiation exposure. He received peripheral blood stem cell transplantation on days 6 and 7. Endotracheal intubation under sedation was introduced on day 10 because of gradual worsening in the patient's respiratory status and in preparation for the future deterioration in the patient's general condition. Despite the intensive care for his symptoms,

exudation from the skin and diarrhea had got worse day by day. He had died on day 82. Details of the clinical course were documented previously.<sup>7)</sup>

Daily volumes of fluid discharge are shown in Fig. 1. Clinical course related to gastrointestinal injuries is summarized below. Mild diarrhea was observed for the first two days after the accident as a symptom of prodromal syndrome and, on day 26, severe diarrhea with bilious watery stool started as a symptom of radiation-induced gastrointestinal syndrome. The volume of watery stool increased to 3500 mL per day on day 39. Bloody stool was observed starting on day 45. The volume of bloody stool increased day by day. Continuous arterial infusion of vasopressin was started from

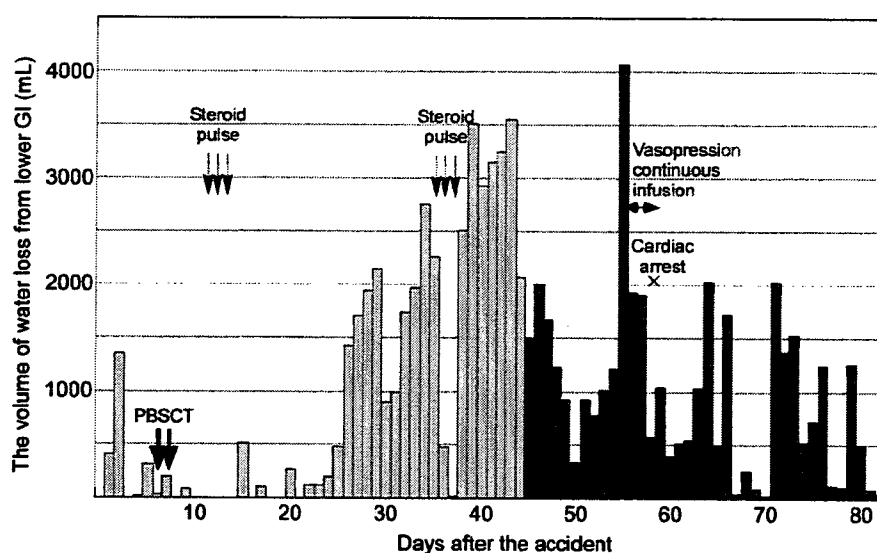


Fig. 1. Daily change in the volume of fluid loss from lower gastrointestinal tract. Light gray bars represent watery diarrhea. Bloody stool, shown by dark gray bars, started on day 45. Major treatments and events are indicated. Abbreviation: PBSCT = peripheral blood stem cell transplantation.

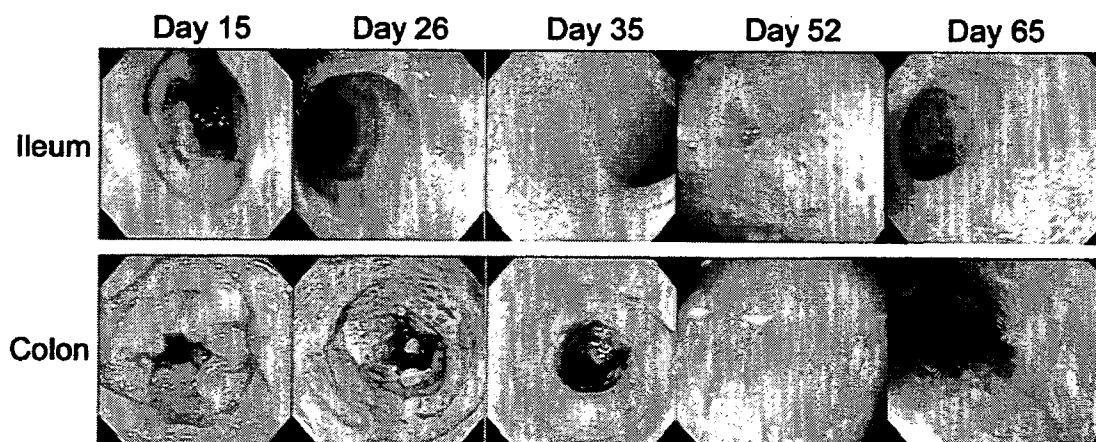
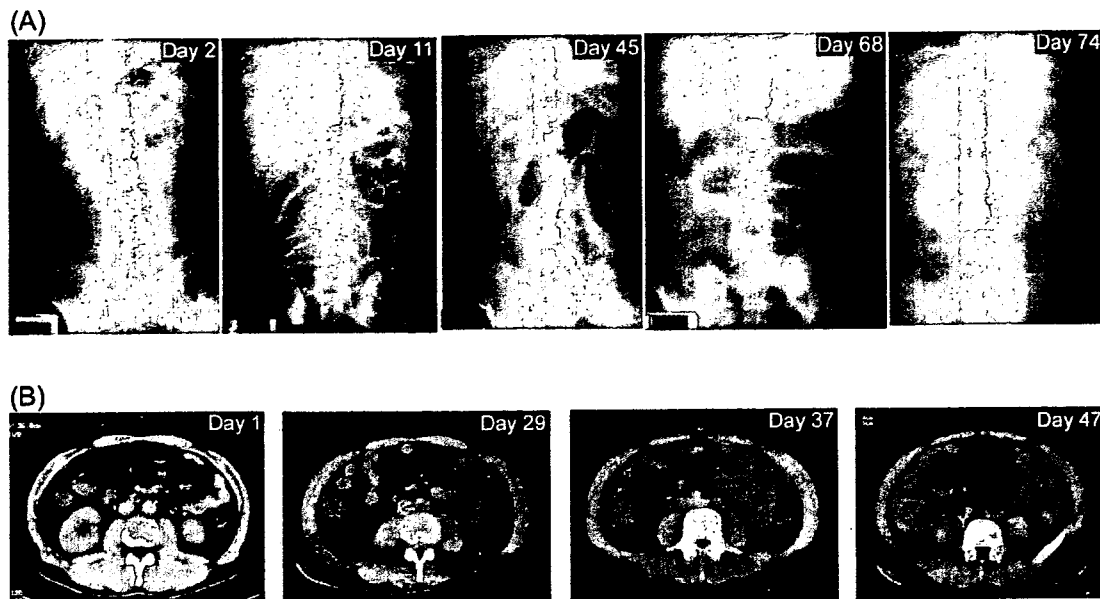


Fig. 2. The appearance of the ileum and colon by colonoscopy. The mucosa appeared almost normal on day 15, but the spots were observed on day 26. After day 35, no mucosa was observed in either the ileum or the colon. The number of bleeding sites thereafter increased.

an indwelling catheter in the superior mesenteric artery on day 55. The volume of bloody stool decreased from 4000 mL to 2000 mL per day by continuous vasopressin infusion. Vasopressin infusion, however, was discontinued on day 58, when there was a cardiac arrest of undetermined etiology. The patient was successfully resuscitated at that time. The

volume of melena suddenly decreased on day 67, implying a blood clot-induced intestinal obstruction. A series of high-pressure enemas was tried thereafter but failed to relieve the obstruction. After the episode of cardiac arrest, multiple organ hypoperfusion developed, and finally the patient died of MOF on day 82.



**Fig. 3.** Abdominal radiographs (A) and abdominal CT images (B). (A) The radiograph on day 2 appeared almost normal. Ileac gas was prominent on day 11, but Kerckring's folds were observed. On day 45, the small intestine was swollen without Kerckring's folds. The abdominal opacity decreased and the small intestine was more swollen with intestinal gas on day 68, when melena suddenly stopped. The decreased opacity of the abdomen represented the increased ascites and intestinal bleeding. On day 74, the decrease in the abdominal opacity was more prominent, and the ileac gas decreased. (B) Only the wall of the ascending colon was thickened, but the small intestine and the transverse and descending colon appeared normal on day 1. Thickening of the entire intestinal wall with the contents of fluids and air was observed on day 29. The wall thickening and the fluid collection were more prominent on day 37. The arrowhead indicates thickening of the colon wall and mesentery with intestinal fluid collection. Ascites appeared on day 47. The intestinal wall thickening was generally decreased, but the wall of the ascending colon remained thickened.

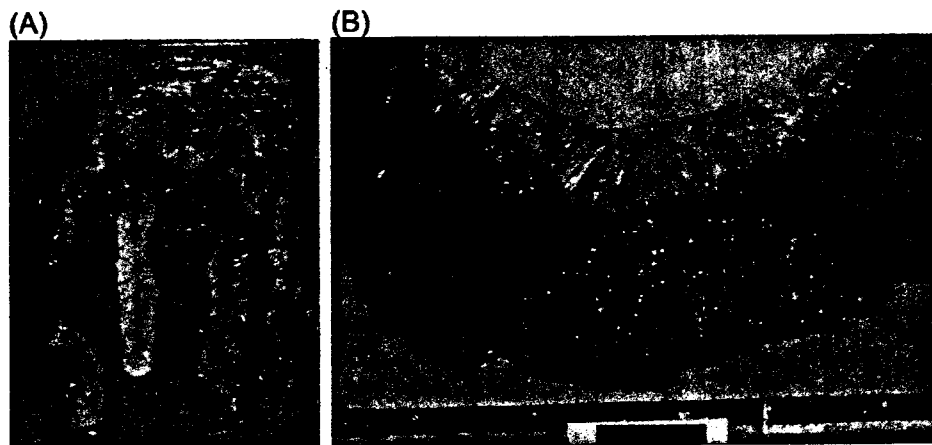


**Fig. 4.** The macroscopic findings at autopsy. (A) The macroscopic appearance of the small intestine and the colon, which was swollen and contained a large number of blood clots *in situ*. Erosive lesions were observed in the mucosa of the entire intestine. (B) Magnified view of the ileum. Segmental intestinal bleeding is present.

## RESULTS

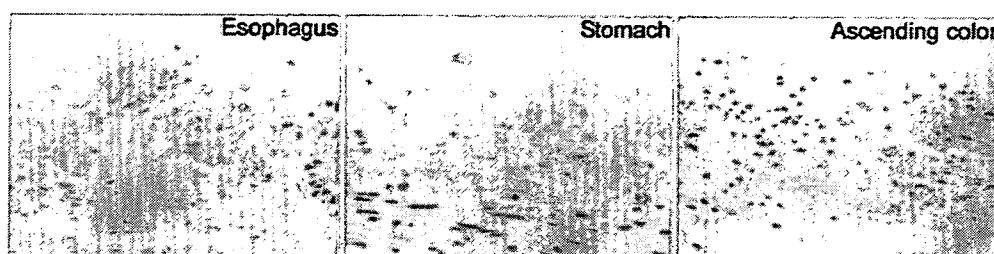
### Endoscopic findings

Figure 2 illustrates representative serial endoscopic findings in the ileum and colon from days 15 to 65. The patient had his first colonoscopy on day 15, revealing bilious intestinal contents with no signs of mucosal injection or loss. The second colonoscopy was performed on day 26, since the volume of watery stool increased suddenly to 1433 mL a day. There were brown spottings on the sigmoid and descending colon, and the surface was covered with a pseudo-membranous white coat on the transverse and ascending

colon. The mucosa was generally injected, but the edematous appearance was slightly relieved compared with the findings of the previous colonoscopy. The ileal mucosa was totally lost and presented a so-called lead-pipe appearance on day 35. Colonoscopy performed on day 52 revealed that the ileal mucosal spots had increased in number. On day 65, the colon contained a large number of blood clots, which occupied the majority of the intraluminal space of the colon. Areas of patchy bleeding were observed on the ileal wall.

### Radiological findings

Representative abdominal radiographs and CT images were shown in Fig. 3. CT images revealed that the wall of



**Fig. 5.** Microscopic findings of the mucosa of esophagus, stomach, and ascending colon, by hematoxylin and eosin staining. In the esophagus, few squamous cells were observed and the esophageal glands were partly remnant. But, no epithelial cells were remnant in the mucosa of the stomach or ascending colon.

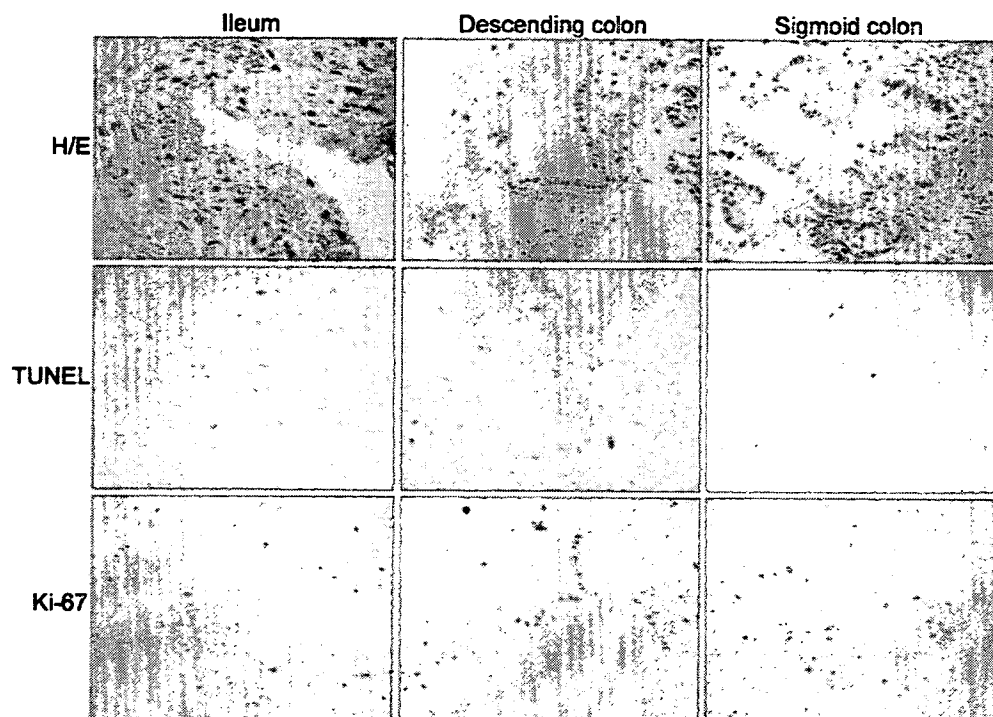


**Fig. 6.** Hematoxylin and eosin staining, TdT-mediated dUTP-biotin nick end labeling (TUNEL), and anti-Ki-67 immunostaining of the ileum, descending colon, and sigmoid colon. The cells positive for TUNEL, representing apoptotic cells, were hardly seen in the ileum, descending colon, or sigmoid colon. Anti-Ki-67 immunostaining revealed that there were no mitotic cells in the ileum, but 71% and 35% of the epithelial cells were positive for Ki-67 antigen in the descending and sigmoid colon, respectively.



the ascending colon was swollen and edematous as early as day 1, but there were no specific findings in other sites of the gastrointestinal tract (Fig. 3). An abdominal radiograph on day 2 was almost normal. On day 11, the dilated small bowel with prominent ileac gas was observed. The wall thickening of the entire gastrointestinal tract increased thereafter, suggesting the presence of inflammation such as infectious enteritis and radiation-induced enteritis. The volume of ascites was estimated to be 2500 mL by abdominal ultrasonography on day 42. The ileum was partly dilated with gas on day 45 on the abdominal radiograph. The attenuation level was increased in the whole abdomen, which suggested an increased volume of ascites. On day 68, dilatation of the ileum filled with gas was more remarkable. But on day 74, bowel gas decreased and the attenuation level was more prominent in the whole abdomen, which was a so-called gasless abdomen.

#### Postmortem examination findings

Postmortem examination was performed 4 hours after the patient's death. The stomach, jejunum, and ileum were filled with coagulated bloody content and were prominently congested at autopsy (Fig. 4). The stomach and small intes-

tine contained 2040 g and 2680 g of clots, respectively. Throughout the gastrointestinal tract, the mucosal epithelial cells were ablated, mucosal congestion was seen, and bleeding occurred in many places (Fig. 4). Dyskaryotic cells proliferated in the stroma, and fibrotic changes in the submucosa and smooth muscle degeneration were also observed (Fig. 5 and 6).

A few squamous cells were observed in the esophagus, and the esophageal glands were partly remnant. No epithelial cells were remnant from the stomach to the ascending colon, but a few epithelial cells were observed in the descending colon, sigmoid colon, and rectum (Fig. 5 and 6). In the colon, fibrotic change was seen in the lamina propria, which was covered partially with regenerating epithelial cells. The proliferative status of the epithelial cells in the descending and sigmoid colon were examined by anti-Ki-67 immunostaining (Fig. 6). In the descending and sigmoid colon, 71% and 35% of the epithelial cells were positive for Ki-67 immunostaining, respectively. In addition, the activity of the apoptotic cascade in these epithelia was also examined by TdT-mediated dUTP-biotin nick end labeling (TUNEL) and anti-p53 and anti-p21 immunostaining (Figs. 6 and 7B). Apoptotic cells were not observed in these epi-

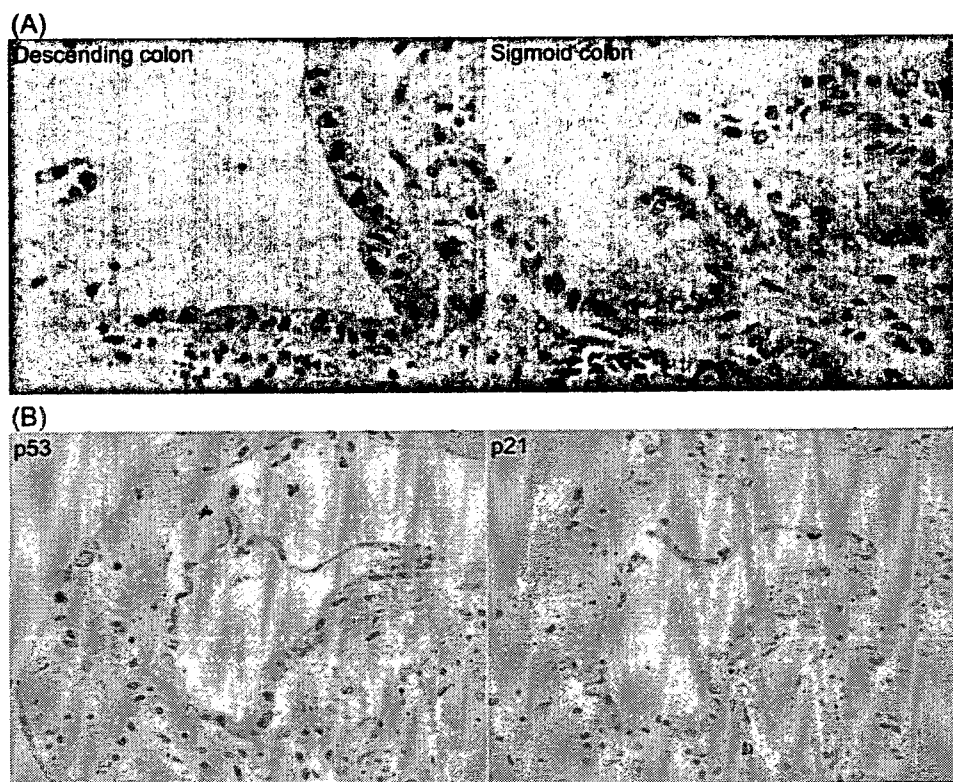


**Fig. 7.** (A) Magnified view of hematoxylin and eosin staining of the descending and sigmoid colon. Dyskaryosis was more severe in the descending colon than in the sigmoid colon. (B) Anti-p53 and anti-p21 immunostaining of the descending colon. Staining of the epithelial cells was negative for both.

**Table 1.** The estimated absorbed dose by the gastrointestinal tract

Site	Gamma ray (Gy)	Neutron beam (Gy)	Total dose (Gy)	Equivalent dose <sup>a</sup> (GyEq)
Esophagus	8.8–13.9	1.1– 4.6	9.8–18.5	10.6–21.7
Stomach	9.1–25.1	1.9–16.3	11.0–41.3	12.3–52.7
Small intestine	7.2–29.2	2.1–19.0	9.3–48.2	10.7–61.6
Ascending colon	20.9–33.8	15.1–24.5	36.0–58.4	46.6–75.5
Descending colon	8.4–13.7	1.0– 7.6	9.5–21.2	10.2–26.5
Sigmoid colon	10.3–12.5	3.3– 6.7	13.7–19.2	16.0–24.0

*Notes.* The absorbed dose of each segment of the gastrointestinal tract was estimated by projecting CT images acquired after the patient's hospitalization on the phantom model of the dose distribution.<sup>17)</sup>

<sup>a</sup>The equivalent doses were calculated assuming the relative biological effectiveness of the neutron beam as 1.7 according to the report by National Institute of Radiological Sciences.<sup>6)</sup>

thelia, because the epithelial cells were negative for TUNEL as well as for both p53 and p21 immunostaining. On the ileal mucosa, neither mitotic cells nor apoptotic cells were seen. Comparing the epithelial appearance of the descending colon and the sigmoid colon, the dyskaryosis was more severe in the epithelial cells of the former (Fig. 7A). The absorbed dose of each segment of the gastrointestinal tract was estimated from the phantom model of the dose distribution and CT images, as shown in Table 1. Although the methods of estimating these absorbed doses have uncertainties, pathological changes of the radiation-induced tissue injuries in each segment of the gastrointestinal tract appeared to be dose-dependent in general.

Major findings other than those for the gastrointestinal systems were previously reported elsewhere.<sup>8)</sup>

## DISCUSSION

We report the clinical course and the pathological features of the gastrointestinal tract in a severely radiation-exposed victim of the 1999 Tokai-mura criticality accident. At 82 days after the accident, the patient died of MOF caused by acute radiation syndrome, especially by gastrointestinal syndrome due to radiation exposure.

Abdominal radiograph revealed enlargement of the small intestine on day 11. Since then, the small intestine was consistently swollen, and Kerckring's folds were not observed on the abdominal radiograph. This suggested peristaltic dysfunction, although no clinical signs of such abnormalities were seen. The mucosa of the colon, however, appeared almost normal during the colonoscopy on day 15. These observations together indicate that functional disruption of the gastrointestinal tract preceded the morphological changes. Watery diarrhea started on day 26, and on the same day the second colonoscopy revealed multiple spotty bleeding on the mucosa of the colon. Thereafter, the symptom of watery diarrhea deteriorated and bloody diarrhea also developed. These observations can be interpreted as a collapse in the

absorptive function of the gastrointestinal systems due to radiation exposure, with no obvious recovery process. Total depletion of the mucosa, which was observed both during the colonoscopy and at autopsy, appeared to cause these gastrointestinal malfunctions.

There are some previous reports on autopsy results after acute radiation exposure accidents. In the Los Alamos criticality accident of 1946<sup>9)</sup> and in the Norwegian case of <sup>60</sup>Co gamma ray exposure in 1982,<sup>10)</sup> victims were exposed to doses similar to that received by the patient we present here, and they died on the 9th day and 13th day after exposure, respectively (estimated approximate systemic dose of 21 Gy for the Los Alamos case and 10–30 Gy for the Norwegian case). At autopsy, the gastrointestinal epithelium was entirely depleted in those two cases.<sup>9,10)</sup> In general, the patient experiences radiation-induced gastrointestinal syndrome 4–10 days after exposure to a dose in the range of 5–12 Gy.<sup>11)</sup> The Los Alamos and Norwegian cases appeared to present typical clinical courses.

On the other hand, the mucosa of the colon looked almost normal in the patient we treated by the colonoscopy even on day 15. In addition, this patient did not suffer from apparent symptoms of MODS before day 18, when a deep burn developed in the right forearm and was presumed to be the onset of MODS. The reason for this difference is unknown, but the early start of intensive care for this patient might have had a good clinical effect; such care included blood stem cell transfusion on days 6 and 7, prophylactic administration of anti-bacterial, anti-fungal, and anti-viral drugs started on day 2, selective digestive tract decontamination, and intravenous administration of high-dose L-glutamine. Ziegler *et al.* suggested that infection might alter gut barrier function to facilitate translocation of bacteria and absorption of endotoxin.<sup>12)</sup> Inflammation cascade following such major stress contributes to a patient's susceptibility to MODS.<sup>2,4)</sup>

Many other radiation accident victims who received a systemic dose of greater than 10 Gy are reported to experience similar clinical courses of gastrointestinal malfunctions.

These symptoms included nausea, vomiting, and mild diarrhea shortly after the exposure, with no obvious deterioration for several days. Thereafter, the symptoms deteriorated progressively to watery diarrhea and bloody stool, resulting in MODS. The diminished barrier function of the gastrointestinal tract is associated with systemic infection or MOF after acute radiation exposure, as is in the case of trauma or skinburns.<sup>3,12-15)</sup>

The systemic radiation dose was inhomogeneous. The dose to the ascending colon was assumed to be highest among segments of the gastrointestinal tract, because the patient was irradiated from the right-anterior direction from the detailed inquiry about the situations and the postures of each victims at the accident.<sup>16-18)</sup> The severity of the radiation damage to the gastrointestinal tract in the patient presented here depended on the absorbed dose (Figs. 5 and 6 and Table 1). Total depletion of the epithelial cells in the ileum and ascending colon indicates high-dose radiation, whereas the mucosa in the esophagus, descending colon, and sigmoid colon was less damaged because of the relatively lower radiation dose. At autopsy, the epithelial cells were positive for Ki-67 staining and negative for both p51 and p21 immunostaining in the descending and sigmoid colon, implying active proliferation of the epithelial cells without activation of the apoptotic cascade (Figs. 6 and 7B). This is interpreted as the process of tissue recovery of the colon epithelium from radiation injury. Pathologically, the absorbed dose in the descending colon was speculated to be higher than that in the sigmoid colon, because the rate of Ki-67-positive epithelial cells was higher and dyskaryosis of the epithelial cells was more severe in the descending colon (Fig. 7A). These observations did not appear to reflect the estimated absorbed dose shown in Table 1 (10.7–25.2 GyE in the descending colon vs. 16.0–24.0 GyE in the sigmoid colon). Possible explanations for this include: (a) the inherent uncertainties of absorbed-dose estimation;<sup>6,17)</sup> (b) the posture-related differences in the positions of the descending and sigmoid colon in the abdomen between the time of the accident and that of the CT examination used for calculation of the absorbed dose of each gastrointestinal segment; (c) the location on the colon of the tissue sample used for the pathological evaluations. However, pathological findings in terms of tissue injury caused by acute radiation exposure generally correlated well with the estimated absorbed dose of each segment of the gastrointestinal tract.

When a person is exposed to radiation exceeding the dose at which bone marrow death occurs, bone marrow or stem cell transplantation is generally considered.<sup>1)</sup> For many radiation victims, however, even successful bone marrow or stem cell transplantation would not have enabled them to survive acute radiation syndrome.<sup>7)</sup> Those patients died of MOF with severe gastrointestinal syndrome, as far as the dose was not sufficient to cause radiation-induced central nervous system or myocardial injuries. Moreover, radiation

accidents themselves are rare. Accordingly, it is quite important to describe both the clinical course and the pathological confirmation and to confirm the pathology in order to assess the radiation effects on the gastrointestinal systems. In this respect, our report is unique in its focus on the clinical course and the pathological features of the gastrointestinal function.

In conclusion, the epithelial cells in the stomach, ileum, and ascending colon were totally depleted, but a small portion of the epithelial cells was remnant in the esophagus, descending colon, sigmoid colon, and rectum at autopsy. The degree of radiation injury of the gastrointestinal tract in this patient differed pathologically by the position in the abdomen, depending possibly on the radiation dose. These findings we presented here in this report have not been described *in vivo* in the previous literature, although it is a well-known fact that the whole body radiation dose is inhomogeneous in the victim of an accident of high-dose radiation exposure. Detailed inquiry about the situations at the Tokai-mura criticality accident enabled us to specify the radiation dose absorbed in each segment of the gastrointestinal tract in this patient and to clarify the correlation between the absorbed dose and the severity in the gastrointestinal damages. In this point of view, detailed description of the patient's course contributes to an understanding of the fundamentals of acute radiation injuries and to clinical decision-making for the treatment of such patient.

## ACKNOWLEDGMENTS

Written informed consent to publish the patient's data including descriptions, radiographs, and photographs was obtained from the patient's family.

## REFERENCES

1. Browne, D., Weiss, J. F., MacVittie, T. J. and Pillai, M. V. (1992) Protocol for the treatment of radiation injuries. *Adv. Space Res.* **12**: 165–168.
2. Akashi, M. (2005) Role of infection and bleeding in multiple organ involvement and failure. *BJR Suppl.* **27**: 69–74.
3. Monti, P., Wysocki, J., van der Meeren, A. and Griffiths, N. M. (2005) The contribution of radiation-induced injury to the gastrointestinal tract in the development of multi-organ dysfunction syndrome or failure. *BJR Suppl.* **27**: 89–94.
4. Riedemann, N. C., Guo, R. F. and Ward, P. A. (2003) Novel strategies for the treatment of sepsis. *Nat. Med.* **9**: 517–524.
5. International Atomic Energy Agency. (2000) IAEA reports on Tokaimura accident. International Atomic Energy Agency. *Health Phys.* **78**: 231.
6. National Institute of Radiological Sciences, Final report on dose estimation for three victims of JCO accident. Ed. K. Fujimoto. NIRS, Chiba, 2002.
7. Chiba, S., Saito, A., Ogawa, S., Takeuchi, K., Kumano, K., Seo, S., Suzuki, T., Tanaka, Y., Saito, T., Izutsu, K., Yuji, K., Masuda, S., Futami, S., Nishida, M., Suzuki, G., Gale, R. P.,

- Fukayama, M., Maekawa, K. and Hirai, H. (2002) Transplantation for accidental acute high-dose total body neutron- and gamma-radiation exposure. *Bone Marrow Transplant.* **29**: 935–939.
8. Uozaki, H., Fukayama, M., Nakagawa, K., Ishikawa, T., Misawa, S., Doi, M. and Maekawa, K. (2005) The pathology of multi-organ involvement: two autopsy cases from the Tokai-mura criticality accident. *BJR Suppl.* **27**: 13–16.
  9. Goans, R. E. and Wald, N. (2005) Radiation accidents with multi-organ failure in the United States. *BJR Suppl.* **27**: 41–46.
  10. Reitan, J. B., Brinch, L. and Beiske, K. (2005) Multi-organ failure aspects of a fatal radiation accident in Norway in 1982. *BJR Suppl.* **27**: 36–40.
  11. Roy, L., Bertho, J. M., Souidi, M., Vozenin, M. C., Voisin, P. and Benderitter, M. (2005) Biochemical approach to prediction of multiple organ dysfunction syndrome. *BJR Suppl.* **27**: 146–151.
  12. Ziegler, T. R., Smith, R. J., O'Dwyer, S. T., Demling, R. H. and Wilmore, D. W. (1988) Increased intestinal permeability associated with infection in burn patients. *Arch. Surg.* **123**: 1313–1319.
  13. Goris, R. J., te Boekhorst, T. P., Nuytinck, J. K. and Gimbere, J. S. (1985) Multiple-organ failure. Generalized autodestructive inflammation? *Arch. Surg.* **120**: 1109–1115.
  14. Ryan, C. M., Yarmush, M. L., Burke, J. F. and Tompkins, R. G. (1992) Increased gut permeability early after burns correlates with the extent of burn injury. *Crit. Care Med.* **20**: 1508–1512.
  15. Baue, A. E. (1993) The role of the gut in the development of multiple organ dysfunction in cardiothoracic patients. *Ann. Thorac. Surg.* **55**: 822–829.
  16. Ishigure, N., Endo, A., Yamaguchi, Y. and Kawachi, K. (2001) Calculation of the absorbed dose for the overexposed patients at the JCO criticality accident in Tokai-mura. *J. Radiat. Res. (Tokyo)*, **42** Suppl: S137–148.
  17. Endo, A. and Yamaguchi, Y. (2003) Analysis of dose distribution for heavily exposed workers in the first criticality accident in Japan. *Radiat. Res.* **159**: 535–542.
  18. U. S. Environmental Protection Agency, Detailed dose assessment for the two heavily exposed workers in the Tokai-mura criticality accident. [Updated 2006 May 7; cited 2006 Nov 6]. Available from: [www.epa.gov/radiation/docs/assessment/jaeri/EndoA\\_pres10.pdf](http://www.epa.gov/radiation/docs/assessment/jaeri/EndoA_pres10.pdf).

*Received on May 21, 2007*

*Revision received on July 9, 2007*

*Accepted on July 31, 2007*

*J-STAGE Advance Publication Date: October 12, 2007*

## Bloom's Syndrome Helicase and Mus81 are Required to Induce Transient Double-strand DNA Breaks in Response to DNA Replication Stress

Tsutomu Shimura<sup>1,2</sup>, Michael J. Torres<sup>1</sup>, Melvenia M. Martin<sup>1</sup>  
V. Ashutosh Rao<sup>1</sup>, Yves Pommier<sup>1</sup>, Mari Katsura<sup>3</sup>  
Kiyoshi Miyagawa<sup>3</sup> and Mirit I. Aladjem<sup>1\*</sup>

<sup>1</sup>Laboratory of Molecular Pharmacology, Center for Cancer Research, NCI, NIH Bethesda, MD 20892-4255 USA

<sup>2</sup>Department of Pathology Institute of Development Aging and Cancer Tohoku University Seiryomachi, Sendai, Japan

<sup>3</sup>Section of Radiation Biology Graduate School of Medicine The University of Tokyo 7-3-1 Hongo, Bunkyo-ku, Tokyo 113-0033, Japan

Received 24 August 2007;  
received in revised form  
29 October 2007;  
accepted 1 November 2007  
Available online  
13 November 2007

Edited by J. Karn

Perturbed DNA replication either activates a cell cycle checkpoint, which halts DNA replication, or decreases the rate of DNA synthesis without activating a checkpoint. Here we report that at low doses, replication inhibitors did not activate a cell cycle checkpoint, but they did activate a process that required functional Bloom's syndrome-associated (BLM) helicase, Mus81 nuclease and ataxia telangiectasia mutated and Rad3-related (ATR) kinase to induce transient double-stranded DNA breaks. The induction of transient DNA breaks was accompanied by dissociation of proliferating cell nuclear antigen (PCNA) and DNA polymerase  $\alpha$  from replication forks. In cells with functional BLM, Mus81 and ATR, the transient breaks were promptly repaired and DNA continued to replicate at a slow pace in the presence of replication inhibitors. In cells that lacked BLM, Mus81, or ATR, transient breaks did not form, DNA replication did not resume, and exposure to low doses of replication inhibitors was toxic. These observations suggest that BLM helicase, ATR kinase, and Mus81 nuclease are required to convert perturbed replication forks to DNA breaks when cells encounter conditions that decelerate DNA replication, thereby leading to the rapid repair of those breaks and resumption of DNA replication without incurring DNA damage and without activating a cell cycle checkpoint.

Published by Elsevier Ltd.

**Keywords:** BLM; Mus81; ATR, double-strand breaks; replication fork blockage; aphidicolin

\*Corresponding author. E-mail address: aladjemm@mail.nih.gov.

Abbreviations used: APH, aphidicolin; ATM, ataxia telangiectasia mutated; ATR, ATM and Rad3-related; ATRkd, ATR kinase dead; BLM, Bloom; BS, Bloom's syndrome; BSA, bovine serum albumin; BrdU, bromodeoxyuridine; CldU, 5-chloro-2'-deoxyuridine; DMEM, Dulbecco's modified Eagle's medium; DNA-PK, DNA-dependent protein kinase; DNA-PKcs, catalytic subunit of DNA-PK; DSBs, double-strand breaks; FACS, fluorescence-activated cell sorting; FdU, fluorodeoxyuridine; HU, hydroxyurea; IdU, 5-Iodo-2'-deoxyuridine; MEM, Minimum Essential Alpha Medium; NHEJ, non-homologous end-joining; PBS, phosphate-buffered saline; pol  $\alpha$ , polymerase alpha; PCNA, proliferating cell nuclear antigen; RPA, replication protein A; ssDNA, single-strand DNA; WT, wild-type.

### Introduction

Cells are constantly exposed to exogenous radiation and chemicals as well as to endogenous metabolic products that perturb DNA replication. Perturbed replication may lead to mutations or DNA breaks, which cause genomic instability and activate the S-phase checkpoint. This S-phase checkpoint, which is regulated by the ataxia telangiectasia mutated (ATM) and Rad3-related (ATR) and Chk1 kinases, prevents further initiation of DNA replication as long as DNA damage persists.<sup>1</sup> The mechanism by which perturbed replication leads to lesions that are recognized as DNA damage is unclear. It is thought that DNA polymerase collisions or replication fork collapses generate double-strand DNA

breaks (DSBs) that are recognized as a form of DNA damage, but the precise mechanism by which this occurs is poorly understood.

The protein implicated in Bloom's syndrome, BLM, is a member of the RecQ family of DNA helicases. Bloom's syndrome is associated with growth retardation, immunodeficiency, premature aging, and cancer predisposition.<sup>2-4</sup> Cells deficient in BLM exhibit an elevated frequency of sister chromatid exchange,<sup>4</sup> implicating BLM in suppression of homologous recombination. In addition to its role in homologous recombination, BLM plays one or more roles during DNA replication. BLM, which can be found in PML bodies,<sup>5</sup> localizes to sites of unperturbed and perturbed DNA replication (i.e. replication foci)<sup>6,7</sup> and interacts with the single-stranded DNA (ssDNA) binding protein RPA.<sup>8</sup> BLM physically and functionally interacts and co-localizes with Mus81 endonuclease,<sup>9</sup> an enzyme that is involved in the repair of UV damage<sup>10</sup> and intrastrand crosslinks.<sup>11</sup> Cells deficient in BLM display are sensitive to replication inhibition by hydroxyurea (HU) and camptothecin (CPT)<sup>12,13</sup> and exhibit an endogenous level of double-stranded DNA breaks even in the absence of drug treatment.<sup>14</sup> BLM plays a role in facilitating re-start of stalled replication forks following inhibition of DNA replication.<sup>15,16</sup> It was suggested<sup>15,16</sup> that BLM might process stalled replication forks to generate a DNA structure that serves as a substrate for the DNA repair machinery and activates checkpoint signals. Consistent with this suggestion, BLM deficient cells display a discrete replication profile characterized by a global reduced fork velocity and shorter inter-origin distance,<sup>14</sup> suggesting that those hard-to-resolve structures might also occur at low frequency in the absence of replication inhibiting drugs. However, the nature of the lesions generated by BLM and the mechanism by which those lesions are recognized by the DNA repair and cell cycle checkpoint pathways have not yet been elucidated.

Aphidicolin (APH) is a mycotoxin isolated from *Cephalosporium aphidicola* that specifically inhibits the activity of DNA polymerase  $\alpha$  (pol  $\alpha$ ) in eukaryotic cells, but has little effect on RNA, protein, and nucleotide biosynthesis.<sup>17-19</sup> APH forms a ternary complex with pol  $\alpha$  and DNA<sup>20</sup> that only interferes with the elongation step of DNA replication. Thus, APH inhibits progression of S-phase cells, but does not affect cells in G2, M, or G1 phases. High levels of APH inhibit DNA replication and induce an S-phase checkpoint mediated by active Chk1.<sup>1</sup> Low doses of APH, which perturb DNA replication but are below the threshold for checkpoint activation, are not toxic. Because cells rapidly resume replication after APH removal, APH can be used to synchronize cells in early S-phase.<sup>17-19</sup>

This study examines the activities and functions of BLM and Mus81 in cells undergoing perturbed replication in the presence of replication inhibitors. The results show that brief exposure to low non-toxic doses of APH induced transient DNA breaks in BLM-proficient but not in BLM-deficient cells. BLM-proficient, but not BLM-deficient cells also exhibited

dissociation of DNA polymerase  $\alpha$  and proliferating cells nuclear antigen (PCNA) from replication forks. The dissociation of replication proteins from replication forks and the induction of transient DNA breaks occurred without activating a cell cycle checkpoint. Mus81 endonuclease and a functional ATR kinase were also required for induction of APH-induced DNA breaks and unraveling of replication forks. Following the repair of APH-induced breaks, BLM-proficient, Mus81-proficient cells re-established replication forks and resumed DNA synthesis at a slow pace in the presence of APH. BLM-deficient or Mus81-deficient cells, which did not induce transient breaks, exhibited an irreversible replication arrest that eventually leads to stable DNA breaks, activation of the S-phase checkpoint and homologous recombination. These observations suggest that BLM and Mus81 are both required to induce transient DNA breaks in response to stalled replication forks. Those transient breaks, which are formed in an ATR-dependent manner, are likely to serve as intermediates in the pathway that leads to recovery from stalled replication and resumption of replication at a slow pace.

## Results

### Formation of transient APH-induced DSBs and $\gamma$ -H2AX foci requires BLM

The role of BLM in the response to APH-induced replication stress was examined in BLM-deficient fibroblasts (PSNG13) or in BLM-deficient fibroblasts complemented with BLM cDNA (PSNF5; BLM-complemented).<sup>21</sup> A DNA comet assay was carried out under neutral conditions to measure double-strand DNA breaks (DSBs) in these cells (Figure 1). The comet assay showed that DSBs were detected within 10 min after treating BLM-complemented cells with APH, but DSBs were not detected when BLM-deficient cells were treated in the same manner (compare PSNF5 and PSNF13; Figure 1(a), middle panel). Quantification of the comet assay data (50 nuclei per sample) confirmed that exposure to 1 or 10  $\mu$ g/ml APH altered the distribution of comet tail length in BLM-complemented but not in BLM-deficient cells (Figure 1(b)).

The kinetics of DSB formation was examined in APH-treated BLM-deficient and BLM-complemented cells by immunostaining APH-treated cells with antibodies to phosphorylated H2AX ( $\gamma$ -H2AX), a marker for DNA breaks<sup>22,23</sup> (Figure 2). The number of cells exhibiting above-threshold levels of  $\gamma$ -H2AX staining was recorded using Pathway analysis. When cells are exposed to agents that are known to induce DSBs,  $\gamma$ -H2AX appears rapidly and associates with nascent DSBs, forming discrete foci.<sup>22,23</sup> Immunostaining with antibodies that detect  $\gamma$ -H2AX and PCNA, a marker of S-phase, showed that BLM-complemented cells that exhibited PCNA staining induced transient  $\gamma$ -H2AX foci within 10 min of treatment with low

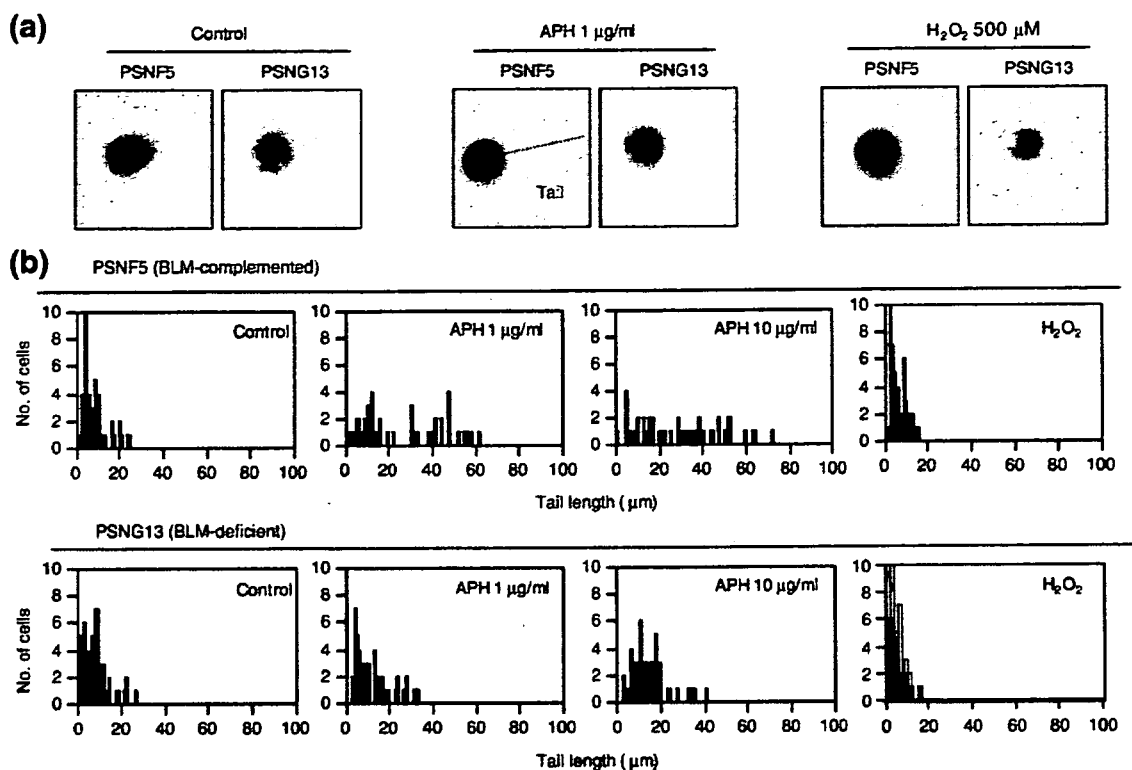


**Figure 1.** DSBs formed after APH treatment evaluated by neutral comet assay. (a) Neutral comet assays were performed using cells exposed to  $H_2O_2$  (500  $\mu M$ ) for 15 min or APH (1  $\mu g/ml$ ) for 10 min as indicated. (b) Average tail length was quantified as described in Methods. BLM-complemented PSNF5 or BLM-deficient PSNG13 cells were used, as indicated. For each data point, 50 nuclei were scored, using data from two independent experiments.

doses of APH (PSNF5; Figure 2).  $\gamma$ -H2AX foci dissociated within 60 min despite the continued presence of low doses of APH (0.5 and 1  $\mu g/ml$ ; Figure 2(a) and (b)). In BLM-complemented PCNA-positive cells treated with 10  $\mu g/ml$  of APH,  $\gamma$ -H2AX foci appeared with similar kinetics, but remained stable beyond 60 min. PCNA-negative cells did not form  $\gamma$ -H2AX foci (data not shown), indicating that APH-induced DSBs only formed during S-phase.

BLM-deficient PCNA-positive cells did not form transient  $\gamma$ -H2AX foci after exposure to 0.5, 1.0 or 10  $\mu g/ml$  of APH (Figure 2; PSNF13); however, a small number of persistent  $\gamma$ -H2AX foci appeared gradually in BLM-deficient cells during exposure to APH for 60 min (Figures 2(b)–(d)). Cell cycle analyses indicated that the fraction of cells in S-phase was similar in BLM-proficient and BLM-deficient cell cultures (Supplementary Data, Figure 1). Therefore, the different response of BLM-complemented and BLM-deficient cells to APH did not result from different kinetics of cell cycle progression in these cells.

We have also investigated the effects of APH on primary normal human fibroblasts (GM00037) and primary Bloom's Syndrome (BS) human fibroblasts (GM01492) (Figure 2(d)). These results confirm that BLM is required for formation of transient APH-induced DSBs. Consistent with this idea, the slow accumulation of persistent DSBs in APH-treated BLM-deficient cells was associated with significantly

lower survival than BLM-proficient cells (Supplementary Data, Figure 2(a)).

Since it was reported that H2AX can be phosphorylated and recruited to DNA damage sites that do not include double-strand breaks,<sup>24,25</sup> it was important to evaluate the breaks we have detected indeed represented double-stranded and not other lesions, such as single-stranded DNA breaks. To insure that the comet assay we have performed above (Figure 1) was specific for DSBs, cells were treated with hydrogen peroxide to generate ssDNA breaks. Cells were then analyzed by neutral comet assays under neutral conditions, that detect only double-stranded DNA breaks, or under alkaline conditions, in which strands unwind and the broken DNA can be detected by comet.<sup>26</sup> When a neutral comet assay was performed, the distribution of DNA tail length was not changed by exposure to hydrogen peroxide (500  $\mu M$  for 15 min; Figure 1(a), right panels); however, when an alkaline comet assay was performed, the distribution of DNA tail length was changed by exposure to hydrogen peroxide (data not shown). These data confirm that exposure to APH induces DSBs in BLM-proficient cells.

#### Formation of APH-induced $\gamma$ -H2AX foci requires Mus81

Previous studies showed that BLM recruits Mus81 nuclease to stalled replication forks and that BLM

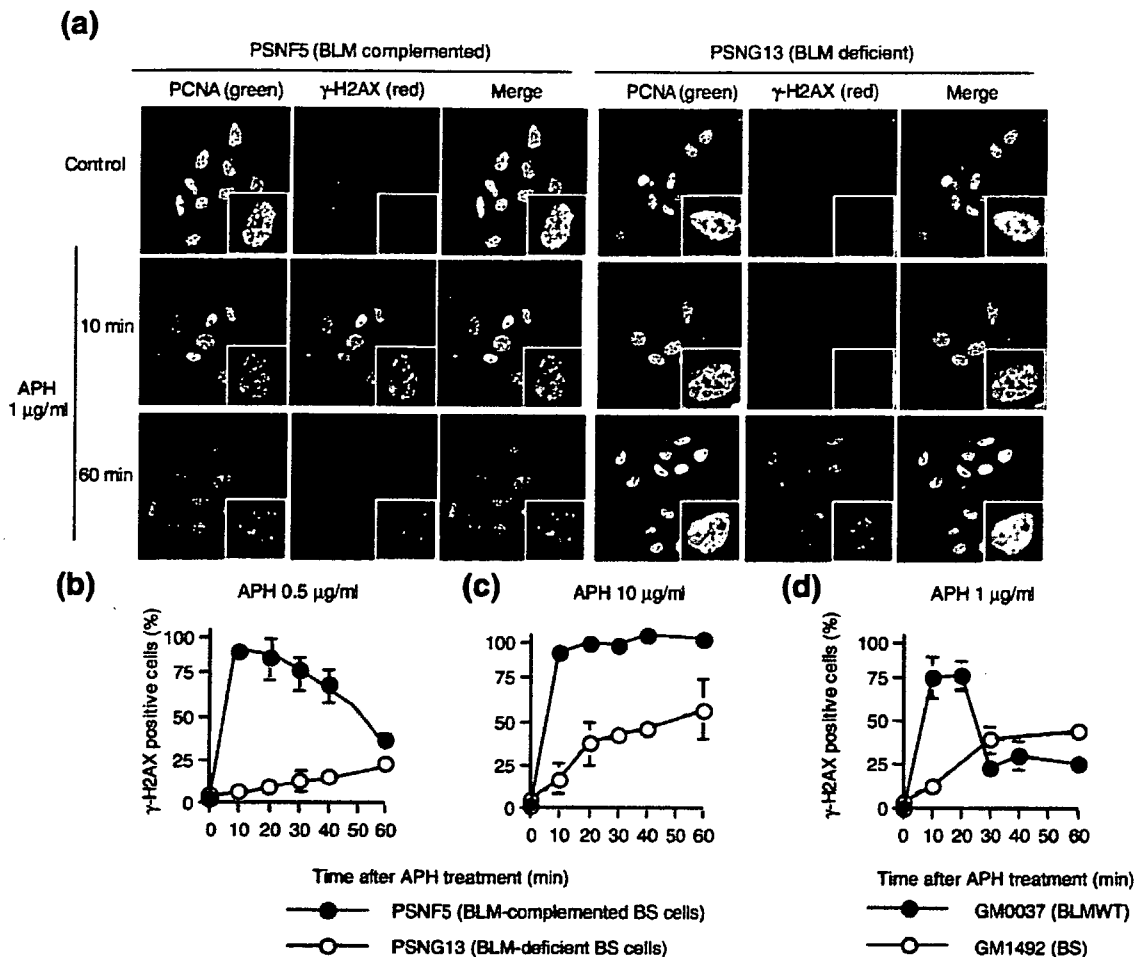


**Figure 2.** BLM-dependent  $\gamma$ -H2AX foci. Cells were treated with APH and then immunostained with PCNA and  $\gamma$ -H2AX. (a) Cells were treated with 1  $\mu$ g/ml of APH for the indicated amount of time and stained for PCNA (green) and  $\gamma$ -H2AX (red) as described in Methods. Insets show images at higher magnification. (b) and (c) The number of  $\gamma$ -H2AX-positive PCNA-positive PSNF5 (filled circles) and PSNG13 cells (open circles) per 100 cells was counted. APH treatment was at the concentration and for the amount of time indicated. (d) The number of  $\gamma$ -H2AX-positive PCNA-positive GM0037 and GM1492 cells per 100 cells was counted. Cells were treated with 1  $\mu$ g/ml of APH for the indicated amount of time. Experiments were repeated three times with independent samples. Error bars represent standard deviations.

enhances the nuclease activity of Mus81.<sup>9</sup> Thus, it seemed possible that Mus81 nuclease might play a role in generating APH-induced BLM-dependent DSBs. Therefore, the kinetics of  $\gamma$ -H2AX foci formation was examined in APH-treated Mus81-proficient HCT116 cells as well as in Mus81-deficient cells (HCT116 Mus81<sup>-/-</sup>) and HCT116 Mus81<sup>-/-</sup> cells complemented with Mus81 cDNA (Figure 3). Since the parental HCT116 cells exhibited a lower threshold for APH sensitivity, a lower concentration of APH (0.5  $\mu$ g/ml) was used in experiments with those cells and their derivatives. In Mus81-proficient and Mus81-complemented cells, transient  $\gamma$ -H2AX foci appeared 10 min after exposure to APH and disappeared about 1 h after the beginning of the exposure, although APH was continuously present in the culture medium (Figure 3(a) and (b)). In contrast, transient  $\gamma$ -H2AX foci were not detected in APH-treated Mus81-deficient cells; those cells slowly accumulated stable DNA breaks. Similarly,

Mus81-proficient cells treated with HU exhibited faster kinetics of accumulation of DNA breaks than Mus81-deficient cells (Figure 3(c)). Consistent with the notion that Mus81 contributes to the processing of stalled replication forks by induction of rapidly repaired DNA breaks, exposure of Mus81-proficient cells to 0.5  $\mu$ g/ml APH did not activate an S-phase replication checkpoint that phosphorylates the Chk1 kinase; Mus81-deficient cells, which did not exhibit transient breaks but exhibited slow accumulation of persistent DNA breaks, had activated the phosphorylation of Chk1 following 30 min exposure to APH (Figure 3(d)).

The above observations demonstrate that Mus81 is required for formation of APH-induced DSBs and APH-induced  $\gamma$ -H2AX foci. Consistent with this, Mus81-deficient cells were hypersensitive to APH (Supplementary Data, Figure 2(b)). These observations suggest that Mus81 contributes to formation of APH-induced BLM-dependent transient DSBs and



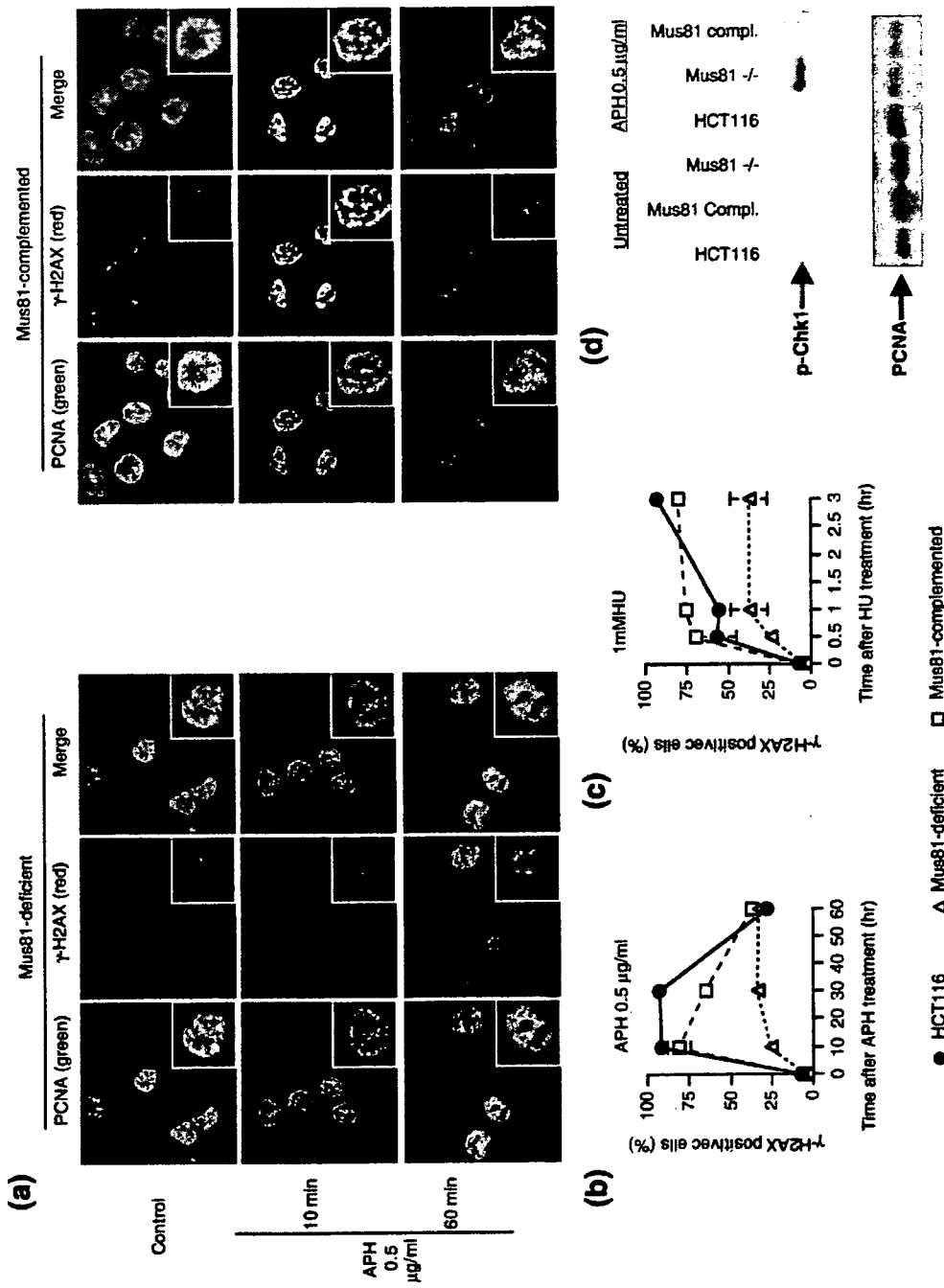


**Figure 3.** Mus81-dependent  $\gamma$ -H2AX foci. Cells were treated with APH and then immunostained with PCNA and  $\gamma$ -H2AX. (a) HCT116 Mus81<sup>-/-</sup> or HCT116 Mus81<sup>-/-</sup> complemented cells were treated with 0.5  $\mu$ g/ml of APH for the indicated amount of time and immunostained for PCNA (green) and  $\gamma$ -H2AX (red), as described in Methods. Insets show images at higher magnification. (b) and (c) The number of  $\gamma$ -H2AX-positive PCNA-positive nuclei per 100 cells was counted. Parental unmodified HCT116 (circles), HCT116 Mus81<sup>-/-</sup> cells (triangles), and HCT116 Mus81<sup>-/-</sup> +Mus81 cells (squares) were treated with APH (b) or HU (c). Each experiment was repeated three times with independent samples. Error bars represent standard deviations. (d) Western blot analysis of phosphorylated Chk1 expression in HCT116 derived cell lines. When treated with 0.5  $\mu$ g/ml of APH for 30 min, only Mus81-deficient cells exhibited staining for p-Chk-1. PCNA was used as a loading control (lower panel).

that this activity is essential for the recovery from transient inhibition of DNA replication.

### Role of ATR in the BLM-dependent response to APH-induced replication stress

BLM is phosphorylated on threonine 99 and 122 by the ATM and ATR kinases.<sup>13,15</sup> The effect of APH on BLM phosphorylation was examined using antibodies to phospho-BLM-T99,<sup>13</sup> considered to be the active form of BLM. Cells were concomitantly stained for PCNA as a marker for S-phase nuclei.

Phosphorylation of BLM, which was absent in untreated cells, was induced in PCNA-positive cells within 10 min of exposure to APH (Figure 4(a)). Cells that did not stain positive for PCNA did not exhibit phosphorylation of BLM (data not shown), suggesting that APH-induced BLM phosphorylation was restricted to the S-phase of the cell cycle. Although phospho-BLM was restricted to PCNA-positive cells, PCNA foci did not co-localize with phospho-BLM. By contrast, phospho-BLM and  $\gamma$ -H2AX co-localized and appeared with similar kinetics (Supplementary Data, Figure 3), suggesting

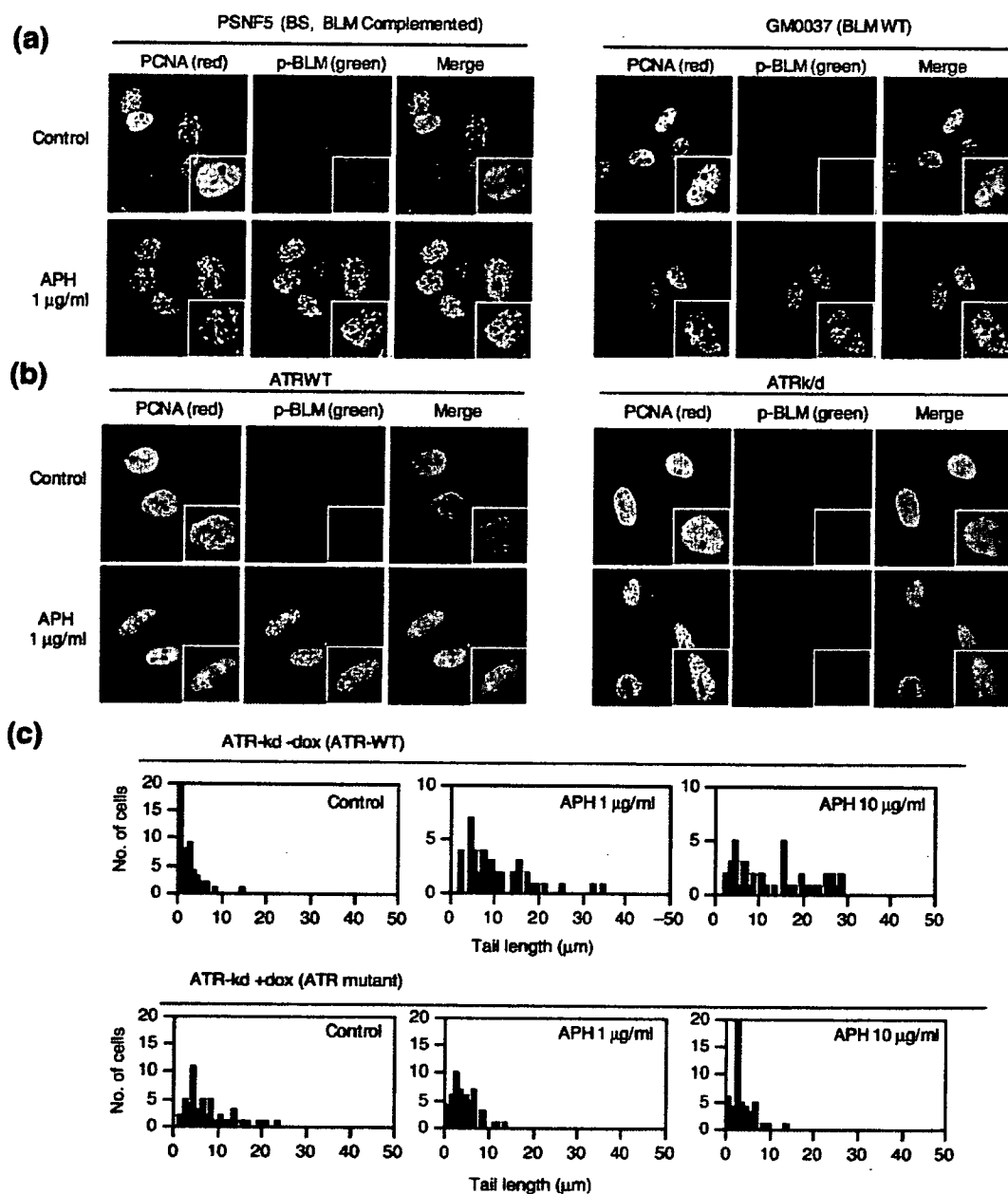


**Figure 4.** Phosphorylation of BLM and formation of DSBs after treatment with low levels of APH. (a) and (b) Cells were treated with 1  $\mu$ g/ml of APH for 10 min and immunostained for PCNA (red) and p-BLM (green). Insets show images at higher magnification. (c) ATR is required for formation of DSBs. The extent of DSB formation was measured by comet assay in cells that contain an active ATR kinase and in cells in which the ATR kinase was inactivated (ATR K/D). Comet assays were performed as described in the legend to Figure 1.

that phospho-BLM accumulates at or near APH-induced DSBs.

BLM phosphorylation was also examined in cells expressing a conditional, doxycycline-inducible dominant-negative kinase-dead form of ATM and Rad3-related kinase (ATRkd). The results showed that APH induced BLM phosphorylation in ATR wild-type (WT) cells but not in ATRkd cells (i.e. pre-treated with 2  $\mu\text{g}/\text{ml}$  of doxycycline for two days to induce ATRkd; Figure 4(b)). By contrast, cells deficient in the PI3 kinase ATM exhibited phosphorylation of BLM with similar kinetics as WT cells (Supplementary Data, Figure 4). These observations suggest that ATR, but not ATM, is required for APH-induced phosphorylation of BLM. To determine if ATR was required for the formation of BLM-induced DNA breaks, we performed comet assays on ATR WT and ATRkd cells. As shown in Figure 4(c), comet tails did

not form in APH-treated ATRkd cells, suggesting that ATR was essential for the formation of APH-induced BLM and Mus81-dependent transient DSBs.

### Effect of APH on elongation of DNA replication in BLM-deficient and BLM-proficient cells

To determine whether the formation and resolution of DSBs after APH treatment play a role in the resolution of stalled replication forks and the resumption of DNA synthesis, we examined replication fork progression in APH-treated BLM-deficient and BLM-complemented cells using a DNA fiber assay.<sup>27</sup> Cells were pulse labeled with 5-Iodo-2'-deoxyuridine (IdU), treated with APH (detected by Cy3; red signal) and labeled with 5-chloro-2'-deoxyuridine (CldU) (detected by Alexa 488; green signal). Figure 5(a) shows that several labeling pat-

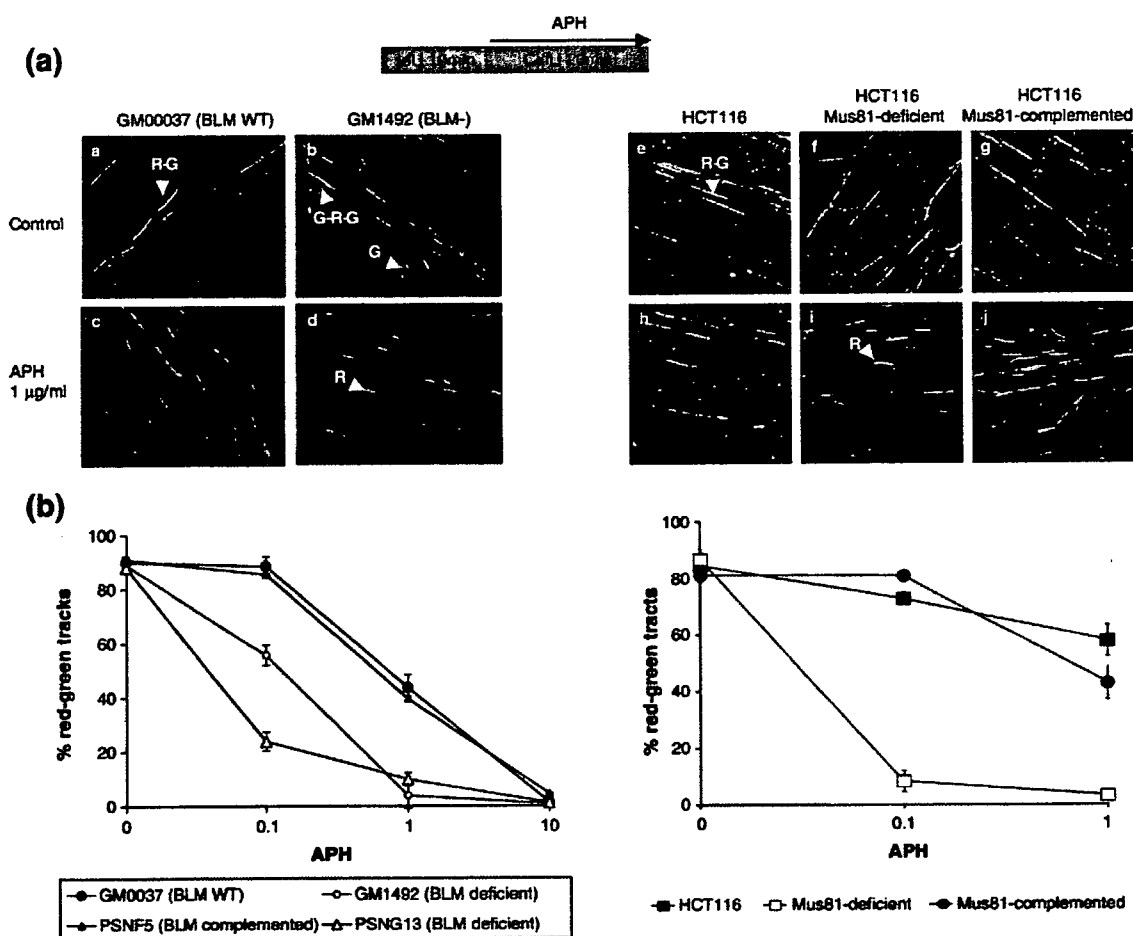


**Figure 5.** Stalled replication forks in cells treated with APH. Replication fork progression was assessed in PSNF5, PSNG13, GM00037, and GM01492 cells. The cell labeling protocol is shown schematically above (a). Cells were labeled with IdU for 10 min. IdU was then washed out and the cells were exposed to APH and CldU for 20 min. IdU was immunodetected by Cy3-labeled antibodies (red color). CldU was detected by Alexa488-labeled antibodies (green color). (a) Representative images of labeled cells are shown. Red-green tracks (R-G), red-only tracks (R), green-only tracks (G), and green-red-green tracks (G-R-G) are indicated by arrowheads. (b) Abundance of R-G (elongation), G (initiation) and R (termination/stalling) in GM00037, GM01492, PSNF5, and PSNG13 cells. (c) Abundance of R-G (elongation), G (initiation) and R (termination/stalling) in HCT116, Mus81-deficient and Mus81-complemented HCT116. Experiments were repeated at least three times with independent samples. Standard deviations are in parenthesis. Experiments were repeated at least three times with independent samples.

terns were observed in these cells: initiation of DNA replication during the second labeling period (in the presence of APH) generated green tracks (G); initiation during the first labeling period generated green-red-green tracks (G-R-G, red signal flanked by two green signals); and initiation before IdU labeling generated unidirectional red-green tracks (R-G). In addition, a few red (R) and rare R-G-R tracks were detected; these are likely due to termination events. The length of DNA fibers can be quantified, providing an alternative to the use of 2D gels, often used in yeast to estimate the extent of initiation and elongation of DNA replication.

The frequency of these different patterns was estimated in BLM-deficient and BLM-complemented cells treated with or without APH. Although BLM deficient cells exhibit a slightly reduced rate of DNA synthesis,<sup>14</sup> those differences were not apparent under the short labeling conditions we have used and the length distributions of replicating DNA tracks were similar in BS and WT cells. However, significant differences were observed after exposure to APH (Figure 5; Supplementary Data, Table 1). In BLM-complemented or BLM-proficient cells (PSNF5 and GM00037), the replicating DNA tracks (green CldU signals in R-G tracks) were significantly shorter in cells treated with APH (Figure 5(a), compare panels a and c); but the frequency of initiation (green-only fibers) was similar in APH-treated and untreated cells (Supplementary Data, Table 1). These results show that replication fork progression was suppressed, but continued at a slow rate, in BLM-proficient cells treated with  $\leq 1$   $\mu\text{g/ml}$  of APH (Figure 5(b), left panel). Treatment with higher doses of APH (10  $\mu\text{g/ml}$ ) resulted in stalling of replication forks and reduced initiation rates in both cell lines.

In BLM-deficient cells (PSNG13 and GM01492), most replication forks were stalled (i.e. R-only tracks) after treatment with  $\leq 0.1$   $\mu\text{g/ml}$  of APH (Figure 5(a), compare panels b and d; Figure 5(b), left panel; Supplementary Data, Table 1) and replication was completely inhibited in cells exposed to higher doses (1–10  $\mu\text{g/ml}$  of APH). Similarly, elongation of replication forks was completely inhibited by APH in Mus81-deficient cells (Figure 5(a), compare panels f and i; Supplementary Data, Table 1), while slow elongation of replication continued in APH-treated Mus81-proficient cells (Figure 5(a), compare panel h to panels i and j; Figure 5(b), right panel). These data confirm that BLM and Mus81 play a role in the response to APH-induced replication stress, allowing slow replication in cells exposed to low levels of APH.

#### **APH-induced disassembly of replication forks requires BLM**

We also investigated the levels and spatial distribution of chromatin-bound PCNA, RPA and DNA polymerases  $\alpha$  and  $\epsilon$  in APH-treated BLM-deficient and BLM-complemented cells. In BLM-proficient cells, the level of total PCNA in the nucleus was not

affected by APH, but levels of chromatin-bound PCNA were lower in APH-treated than in untreated cells. In contrast, the levels of chromatin-bound PCNA were unaffected in APH-treated BLM deficient cells (Figure 6(a)). Consistent with this, we observed lower levels of PCNA in RPA foci after treatment of BLM-proficient cells by APH (Figure 6(b)). We have also observed that DNA polymerase  $\alpha$ -primase leaves chromatin after a short exposure to APH in BLM-proficient, but not deficient cells (Figure 6(c)). By contrast, Replication protein A (RPA), which binds single-stranded DNA, continues to exhibit a focal pattern after treatment with low levels of APH. RPA co-localized with PCNA in untreated cells, but not in cells that were treated with APH for 10 min. RPA foci co-localized with  $\gamma$ -H2AX foci in cells exposed to APH for 10 min (Supplementary Data, Figure 5), suggesting that DSBs were formed in stalled replication factories.

Although PCNA and DNA polymerase  $\alpha$ -primase dissociated from RPA foci in BLM-proficient cells, the distribution of PCNA and DNA polymerase  $\alpha$ -primase was not affected in BLM-deficient cells (Figure 6(b); Supplementary Data, Figure 6). The distribution of pol  $\epsilon$ , which facilitates leading strand synthesis, was not altered by exposure of BLM-deficient or BLM-complemented cells to APH (Figure 6(d)). PCNA co-localized with pol  $\epsilon$  in untreated but not in APH-treated cells, consistent with the depletion of PCNA from chromatin in APH-treated BLM-complemented cells, observed above. These data suggest that BLM facilitates disassembly of replication forks in cells with APH-induced replication stress. RPA and pol  $\epsilon$  remain at replication forks and co-localize with DNA breaks, whereas PCNA and DNA polymerase  $\alpha$ -primase leave replication forks.

## **Discussion**

This study shows that low doses of APH induce DSBs in replicating cells, and that formation of these DSBs requires BLM and Mus81. APH-induced BLM-dependent DSBs are transient and appear to be rapidly repaired by non-homologous end joining (NHEJ),<sup>28</sup> whereas BLM-independent DSBs, which form infrequently with delayed kinetics in APH-treated BLM-deficient cells, are persistent and accumulate irreversibly. In cells that contain functional BLM, Mus81 and ATR, DNA replication proceeds slowly in the presence of low doses of APH following the repair of the transient surge of DSBs. By contrast, in cells deficient in BLM, ATR or Mus81, replication elongation is completely inhibited and cells cannot progress in S-phase. The inability to replicate slowly in the presence of APH is illustrated by the hypersensitivity of those cells to APH. These data suggest that BLM, Mus81 and ATR are required to induce transient DSBs after short exposure to APH. Since cells that are deficient in each of the above components could not induce transient DSBs, it is plausible to assume that all three